JACS
JOURNAL OF THE AMERICAN CHEMICAL SOCIETY
Article
pubs.acs.org/JACS

Highly Durable and Active PtFe Nanocatalyst for Electrochemical Oxygen Reduction Reaction

Dong Young Chung,[†,‡,#] Samuel Woojoo Jun,[†,‡,#] Gabin Yoon,[†,§] Soon Gu Kwon,[†,‡] Dong Yun Shin,[∥] Pilseon Seo,[†,‡] Ji Mun Yoo,[†,‡] Heejong Shin,[†,‡] Young-Hoon Chung,[⊥] Hyunjoong Kim,[†,‡] Bongjin Simon Mun,[▽] Kug-Seung Lee,[△] Nam-Suk Lee,[○] Sung Jong Yoo,[⊥] Dong-Hee Lim,[∥] Kisuk Kang,[†,§] Yung-Eun Sung,[*,†,‡] and Taeghwan Hyeon[*,†,‡]

[†]Center for Nanoparticle Research, Institute for Basic Science (IBS), Seoul 151-742, South Korea

[‡]School of Chemical and Biological Engineering & [§]Department of Materials Science and Engineering, Seoul National University, Seoul 151-742, South Korea

[∥]Department of Environmental Engineering, Chungbuk National University, Chungbuk 361-763, South Korea

[⊥]Fuel Cell Research Center, Korea Institute of Science and Technology, Seoul 136-791, South Korea

[▽]Department of Physics & Photon Science, Ertl Center for Electrochemistry and Catalyst, Gwangju Institute of Science and Technology, Gwangju 500-712, South Korea

[△]Pohang Accelerator Laboratory (PAL) & [○]National Institute for Nanomaterials Technology (NINT), Pohang University of Science and Technology (POSTECH), Pohang 790-784, South Korea

S *Supporting Information*

ABSTRACT: Demand on the practical synthetic approach to the high performance electrocatalyst is rapidly increasing for fuel cell commercialization. Here we present a synthesis of highly durable and active intermetallic ordered face-centered tetragonal (fct)-PtFe nanoparticles (NPs) coated with a "dual purpose" N-doped carbon shell. Ordered fct-PtFe NPs with the size of only a few nanometers are obtained by thermal annealing of polydopamine-coated PtFe NPs, and the N-doped carbon shell that is *in situ* formed from dopamine coating could effectively prevent the coalescence of NPs. This carbon shell also protects the NPs from detachment and agglomeration as well as dissolution throughout the harsh fuel cell operating conditions. By controlling the thickness of the shell below 1 nm, we achieved excellent protection of the NPs as well as high catalytic activity, as the thin carbon shell is highly permeable for the reactant molecules. Our ordered fct-PtFe/C nanocatalyst coated with an N-doped carbon shell shows 11.4 times-higher mass activity and 10.5 times-higher specific activity than commercial Pt/C catalyst. Moreover, we accomplished the long-term stability in membrane electrode assembly (MEA) for 100 h without significant activity loss. From *in situ* XANES, EDS, and first-principles calculations, we confirmed that an ordered fct-PtFe structure is critical for the long-term stability of our nanocatalyst. This strategy utilizing an N-doped carbon shell for obtaining a small ordered-fct PtFe nanocatalyst as well as protecting the catalyst during fuel cell cycling is expected to open a new simple and effective route for the commercialization of fuel cells.

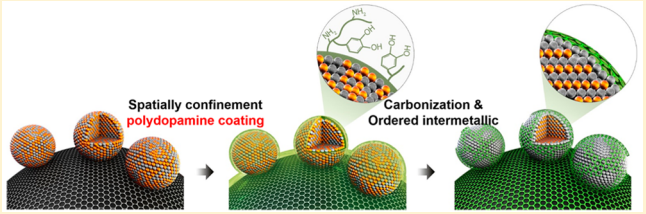

INTRODUCTION

Nanoparticle-based electrocatalysts have been intensively investigated for fuel cell applications over the past decade, mainly motivated by their high mass activity.[1−14] Many research groups have made great effort to utilize the high activity and surface area of nanoparticles (NPs) in order to make a breakthrough for fuel cell commercialization. However, practical use of nanomaterials for fuel cell electrocatalyst was impeded by their low physical and chemical stability. Under the standard fuel cell operating conditions, NPs are often oxidized, dissolved, or detached from the support and agglomerated into larger particles, losing their electrochemical catalytic activity during cycling.[15] Moreover, according to theoretical calculations, the oxidation and dissolution potentials of NPs tend to decrease with their sizes.[16] In these regards, ordered intermetallic NPs are considered as one of the most promising candidates to achieve both high activity and stability in practical fuel cell applications.[17−23] The Sun group reported that the ordered intermetallic PtFe NPs of face-centered tetragonal (fct) structure have superior iron antidissolution property under the acidic fuel cell operating condition. In addition, fct-PtFe NPs show higher activity than the disordered face-centered cubic (fcc) PtFe NPs.[17] The Abruna group reported the superior long-term stability of ordered fct-PtCo NPs,[18] which is attributed to the Pt-rich surface and the strong Pt−Co bonding

Received: September 14, 2015
Published: December 3, 2015

DOI: 10.1021/jacs.5b09653
J. Am. Chem. Soc. 2015, 137, 15478−15485

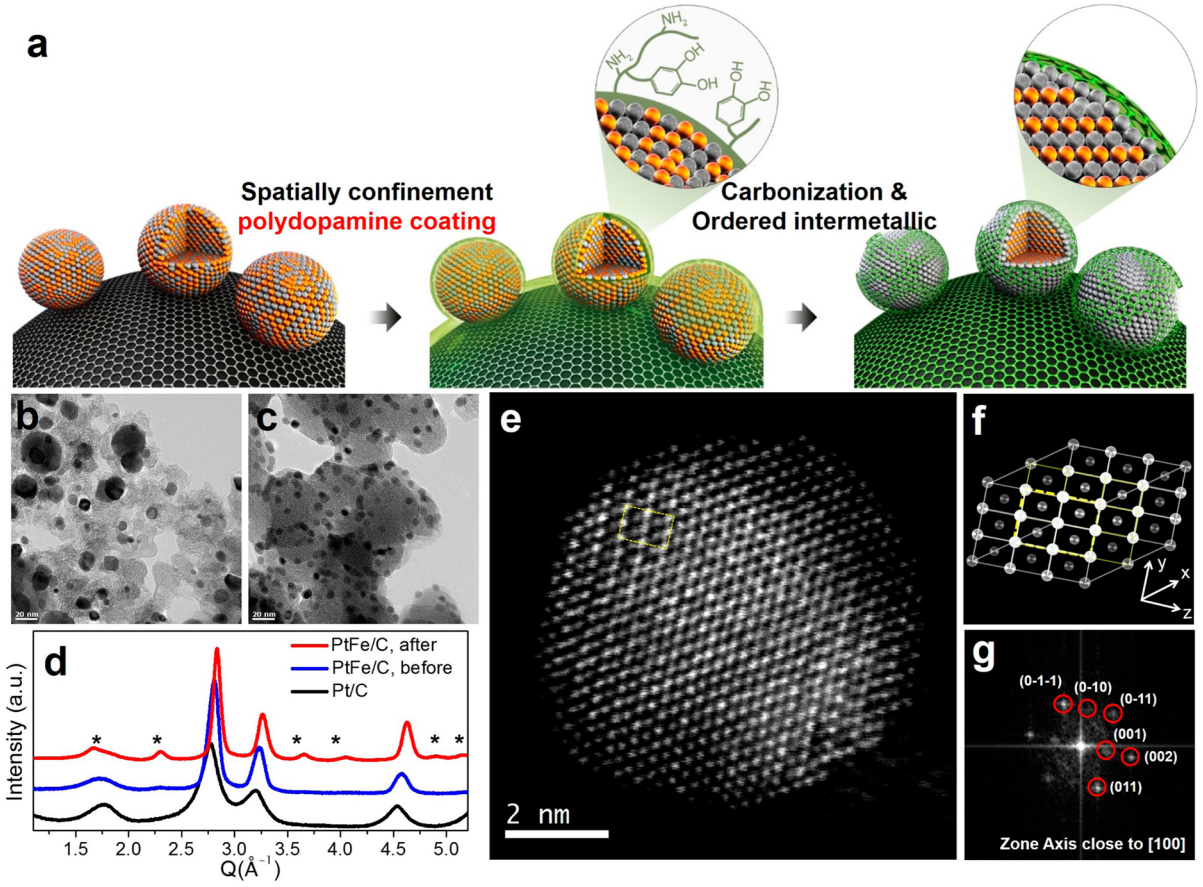

Figure 1. Synthesis of ordered intermetallic fct PtFe/C. (a) Schematic synthesis diagram of carbon-supported and N-doped carbon-coated ordered fct-PtFe NPs. (b-c) TEM images of thermally annealed NPs without (b) and with dopamine coating (c) at 700 °C. (d) HRPD data of carbon-supported pure Pt (Pt/C), PtFe NPs before annealing (PtFe/C, before), and after annealing (PtFe/C, after). (e-g) Cs-corrected HAADF-STEM image of a fct-PtFe NP after annealing (e), a model structure of fct-PtFe structure (f), and a FFT patterns of the image (g). The Pt columns look brighter than the Fe columns due to the Z-contrast.

in the core of the NPs. Despite these advantages, however, the synthesis of small-sized ordered fct-PtFe NPs with high mass activity has been rarely reported thus far. In general, as-synthesized PtFe NPs have disordered fcc structure, and consequently thermal annealing at ~700 °C is necessary to transform them into an ordered fct structure,[24] which inevitably leads to the coalescence of the NPs forming larger and polydisperse NPs. To prevent this coalescence during annealing, protective coating of the NPs with inorganic shells[17,25] or physical barriers[26] has been suggested. However, this approach requires an additional step of removing the coating layer from the surface of the NPs to expose the active sites, which increases time and cost in the production.

In the meantime, there has been another approach to utilize protective coating to enhance the long-term performance of fuel cells. By coating NPs deposited on the support with a protective layer, they can be made more resistive toward detachment and agglomeration, which are the major deactivation mechanisms during fuel cell operation, as mentioned above.[27] So far, various coating layers, including a carbon shell,[28] an inorganic barrier,[29] and graphitic hollow spheres,[30,31] are proposed, and the protective layer-coated NPs show better performance in terms of the long-term stability compared to the uncoated counterparts. Especially, it is known that N-doped carbon has very good affinity to the surface of metal NPs and, thus, stabilizes the small NPs not to agglomerate during the fuel cell operation.[32] However, it was criticized that, although with enhanced stability, the presence of a protective layer can lower the catalytic performance by blocking the active sites and lowering the mass transport rate at the surface of the NPs.

Being inspired by those two different approaches to improve the long-term stability of nanocatalysts, we designed a nanoparticle-based electrocatalyst that combines those approaches together and overcomes their limitations. Herein, we report a synthetic method of highly durable and active PtFe NPs with a very thin "dual purpose" N-doped carbon shell. This carbon shell is *in situ* formed from a polydopamine coating of disordered fcc-PtFe NPs during thermal annealing to transform the NPs into an ordered fct structure. The carbon shell effectively prevents PtFe NPs from coalescence during the annealing so that fct-PtFe NPs as small as 6.5 nm can be obtained. Moreover, by controlling the thickness of the carbon shell at subnanometer scale, the shell also acts as a highly effective protective coating of the NPs during fuel cell cycling while it is still permeable for the reactant molecules and not affecting their electrocatalytic activity. In half-cell and membrane electrode assembly (MEA) tests, our N-doped carbon-coated PtFe NPs show excellent long-term stability for realistic fuel cell application. The origin of the stability of our nanocatalyst is investigated with *in situ* synchrotron X-ray absorption spectroscopy and first-principles calculation model-

DOI: 10.1021/jacs.5b09653
J. Am. Chem. Soc. 2015, 137, 15478−15485

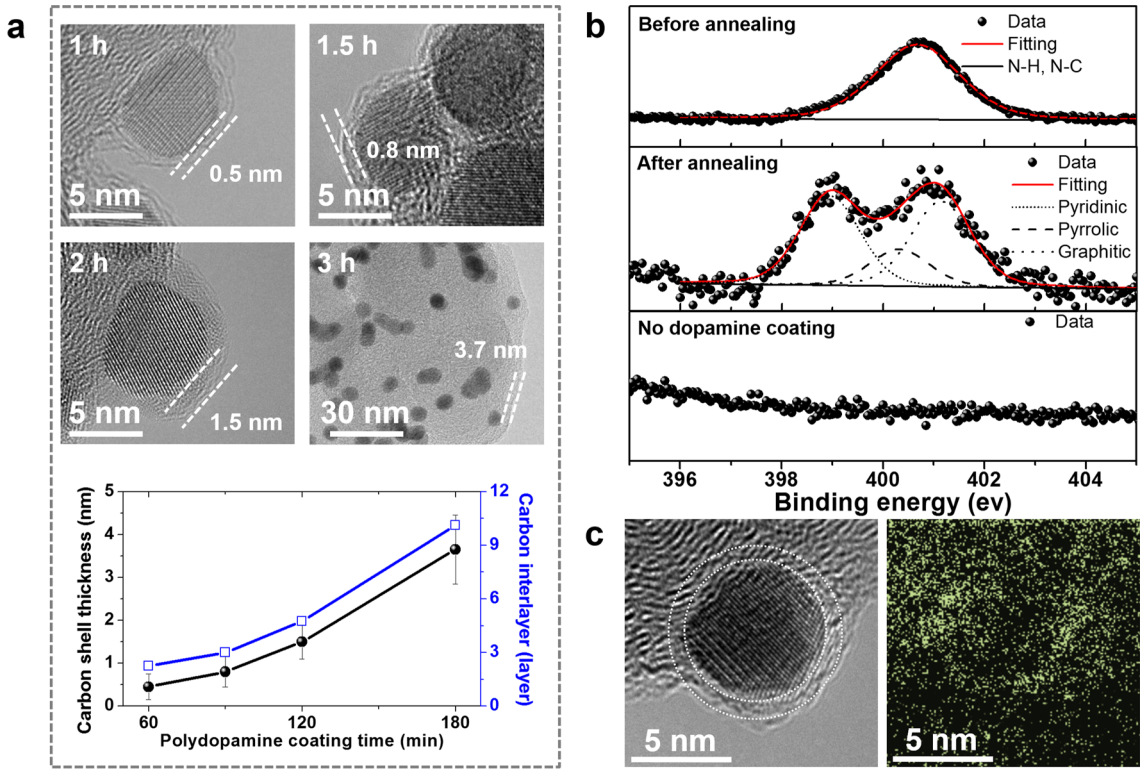

Figure 2. Characterizations of N-doped carbon shells. (a) TEM images of carbon-loaded and N-doped carbon shell-coated PtFe NPs and plots of the shell thickness (number of carbon interlayers) vs polydopamine coating time. (b) HR-PES data around the N 1s core level from PtFe NPs before annealing (top), after annealing (middle), and without dopamine coating (bottom). (c) HR-TEM image of a carbon-supported and carbon shell-coated PtFe NP (left) and its EF-TEM image showing the distribution of nitrogen (right).

ing, and the results confirm the critical importance of the ordered fct structure and the presence of an N-doped carbon shell for the long-term stability.

RESULTS AND DISCUSSION

Preparation of carbon shell-coated PtFe nanocatalyst. The formation process of ordered fct-PtFe NPs with a dual purpose N-doped carbon shell is illustrated in Figure 1a. First, disordered fcc-PtFe NPs are synthesized via the previously reported method using platinum acetylacetonate [$Pt(acac)_2$] and iron pentacarbonyl [$Fe(CO)_5$] as Pt and Fe precursors, respectively (Supporting Information, Figure S1).[33] As-synthesized PtFe NPs are supported on carbon particles and then coated with polydopamine by a treatment with dopamine hydrochloride solution. Thermal annealing of carbon-supported and dopamine-coated fcc-PtFe NPs at 700 °C leads to the formation of atomically ordered fct-PtFe NPs with an N-doped carbon coating. The effect of an *in situ* formed N-doped carbon shell is investigated by performing a control experiment without a dopamine coating. As shown in Figures 1b and 1c, thermal annealing of carbon-supported PtFe NPs (PtFe/C) without a dopamine coating leads to a significant increase in the NP size up to tens of nanometers due to extensive coalescence. On the other hand, 6.5-nm-sized NPs are obtained from thermal annealing of dopamine-coated PtFe/C, which is close to the initial size of the NPs before the annealing (Figure S2), which confirms that the *in situ* formed carbon shell makes the NPs highly resistive toward coalescence. The ordered intermetallic fct structure of PtFe/C after the annealing is confirmed by high resolution powder diffraction (HRPD) in Figure 1d in comparison with PtFe/C before annealing and pure Pt/C. The characteristic superlattice peaks of the ordered intermetallic fct structure appear after the annealing, as marked with asterisks. Also, high angle annular dark field-scanning transmission electron microscopy (HAADF-STEM) and fast Fourier transform (FFT) analysis (Figures 1a–1g) confirm the ordered fct structure of PtFe NPs. In these images, the unit cell projected along the [001] axis shows a periodic line array of Fe columns stacked by Pt columns.

Polydopamine is used as the precursor for *in situ* formation of an N-doped carbon shell.[34] The thickness of the N-doped carbon shell can be precisely controlled by the coating time of polydopamine.[35] TEM data show that the thickness of the polydopamine coating is roughly proportional to the coating time (Figure 2a). In the case of 1 h coating, the carbon shell with average thickness of ~0.43 nm is formed, which amounts to approximately two layers of carbon sheet (Figure S3). In high resolution photoemission spectroscopy (HR-PES) data, the presence of N–C and N–H bonding is confirmed in the N 1s signal from polydopamine-coated NPs before the annealing (Figure 2b). After thermal annealing at 700 °C, carbonization of dopamine takes place and signals from pyridinic (N 1s ~ 399 eV), pyrrolic (N 1s ~ 400 eV), and graphitic (N 1s ~ 401 eV) nitrogen are observed, indicating that dopamine is transformed into an N-doped carbon shell. From a controlled sample without dopamine coating, no nitrogen signal is detected. The ratio of N 1s and Pt 4f signal intensities, which is proportional to the thickness of the dopamine coating of PtFe NPs, is increased with the coating time (Figure S4), further supporting the result from the TEM data. Bright field and energy-filtered TEM (EF-TEM) images in Figure 2c and Figure S5 reveal that

DOI: 10.1021/jacs.5b09653
J. Am. Chem. Soc. 2015, 137, 15478–15485

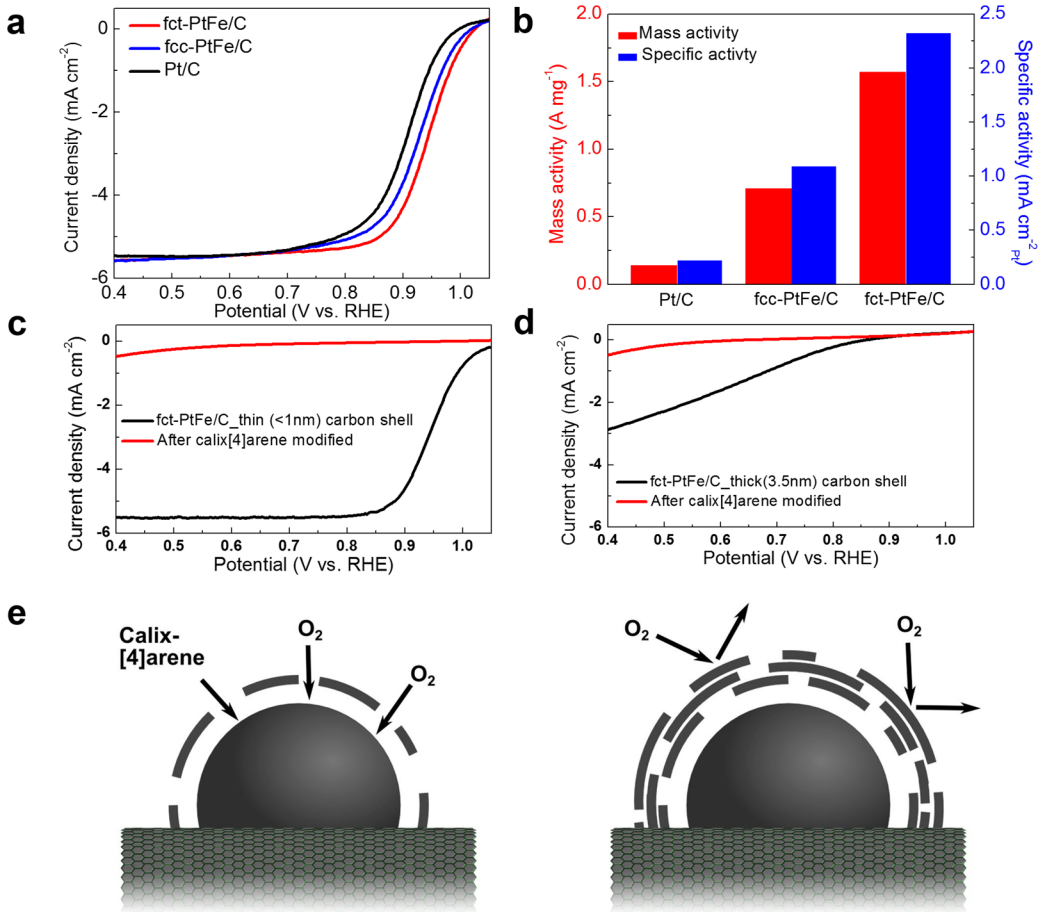

Figure 3. Electrochemical oxygen reduction reaction activity. (a) Oxygen reduction reaction activity of ordered fct-PtFe/C, disordered fcc-PtFe/C, and Pt/C measured using a 1600 rpm rotating disc electrode. (b) Mass and specific activities of the electrodes measured at 0.9 V. (c and d) ORR activity of ordered fct-PtFe nanocatalysts modified with calix[4]arene thiol derivative with thin (c, <1 nm) and thick (d, 3.5 nm) carbon shells. (e) Schematic diagrams of active sites with respect to the carbon shell thickness.

nitrogen is mainly distributed in the carbon shell adjacent to the PtFe NP.

Electrochemical tests of PtFe nanocatalysts. The electrocatalytic properties of N-doped carbon shell-coated ordered fct-PtFe/C nanocatalyst are investigated by performing oxygen reduction reaction (ORR) using a rotating disk electrode. For comparison, disordered fcc-PtFe/C nanocatalyst is prepared by thermal annealing of PtFe NPs at 400 °C instead of 700 °C (Figure S6). Also, commercial Pt/C electrocatalyst is tested as a standard. According to ORR polarization curves in Figure 3a, ordered fct-PtFe/C shows the highest performance followed by disordered fcc-PtFe/C and Pt/C in terms of the half-wave potential. The mass activity of ordered fct-PtFe/C was 1.6 A·mg^{-1}, which is 11.4 times higher than that of Pt/C (0.14 A·mg^{-1}, Figure 3b and Table S1). The specific activity of ordered fct-PtFe/C (2.3 mA·cm^{-2}) is also improved by 10.5 times compared to Pt/C (0.22 mA·cm^{-2}). In order to study the relationship of these enhanced catalytic properties to the ordered fct structure of PtFe/C, various structural analyses are performed. In general, the increase in electrocatalytic activity for ORR is attributed to the change in the oxygen adsorption energy by electronic structure modification[36−38] and geometric effects.[39,40] HR-PES and X-ray absorption near edge structure (XANES) spectroscopy measurements reveal modification of the d-band structure of ordered fct-PtFe NPs compared to pure Pt (Figure S7). In addition, according to HRPD (Figure 1d) and extended X-ray absorption fine structure (EXAFS) analysis (Figure S8 and Table S2), ordered fct-PtFe NPs have smaller lattice constant and shorter Pt−Pt and Pt−Fe bond lengths compared to disordered fcc-PtFe NPs. Combining the electronic structure and strain analysis data, we conclude that ordered fct-PtFe NPs have lower oxygen adsorption energy compared to disordered fcc-PtFe NPs and Pt/C, leading to the enhanced electrocatalytic activity. (For the detailed explanation, see Figures S7 and S8 Supporting Information). Moreover, the lower OH adsorption is supported by the cyclic voltammograms (CV) (Figure S9). The OH adsorption peak is positively shifted significantly in the case of fct-PtFe/C, which suggests low oxygen adsorption intensity. To test the possibility of any contribution of N-doped carbon shell to the catalytic activity, we prepared N-doped carbon shell-coated Pt/C (Figure S10) and tested it under the same conditions as the data in Figure 3a. The result shows negligible effect of the shell on the activity, which confirms that the enhancement in the ORR activity is originated from the ordered fct structure of PtFe NPs.

Recently, it was reported that N-doped carbon-coated metal (Fe and Co) structures showed electrocatalytic activity for ORR.[41,42] Therefore, we investigated whether the observed activity of ordered fct-PtFe/C is originated from the carbon shell or metal core by using calix[4]arene thiol derivative, which is a well-known oxygen inhibitor in ORR due to its strong binding ability to the surface of electrocatalyst with its thiol

DOI: 10.1021/jacs.5b09653
J. Am. Chem. Soc. 2015, 137, 15478−15485

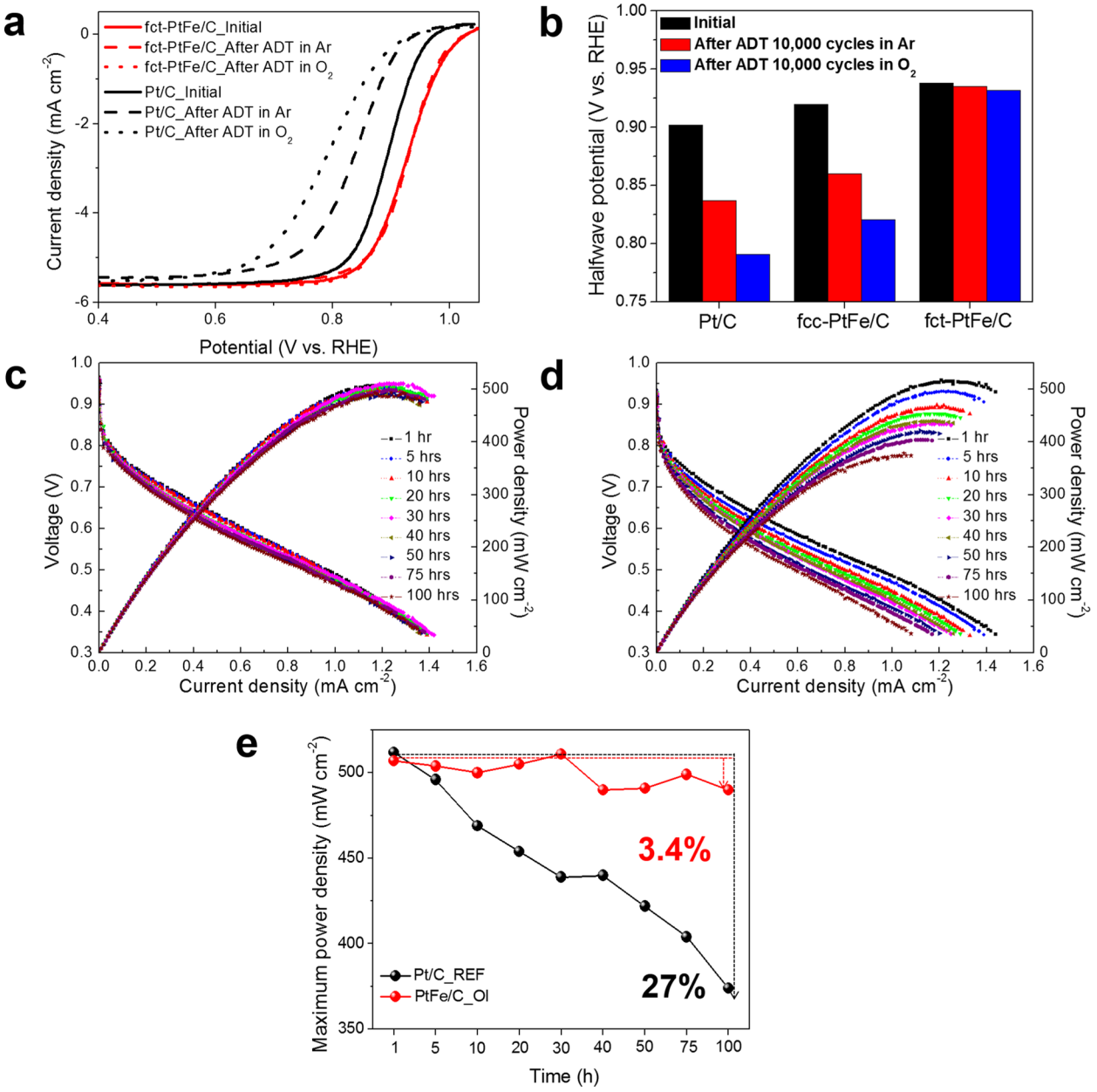

Figure 4. Long-term stability test before and after ADT. (a and b) ORR polarization curves (a) and changes in half wave potentials (b) of Pt/C, fcc-PtFe/C, and fct-PtFe/C before and after ADT of 10,000 cycles. (c–e) Results from 100 h MEA test for fct-PtFe/C (c) and Pt/C (d) and their maximum power density plot as functions of operating time (e).

group.[43,44] In a control experiment, Pt/C modified with calix[4]arene thiol derivative is almost completely deactivated, proving the deactivation ability of this compound (Figure S11). In Figures 3c and 3d, ORR polarization curves before and after calix[4]arene thiol derivative modification are compared for ordered fct-PtFe/C with thin (<1 nm) and thick (3.5 nm) N-doped carbon shells, respectively. In the data from both thin and thick shell samples, the thiol modification leads to deactivation of the catalytic activity, confirming that ORR takes place at the surface of PtFe NPs. At the same time, this result confirms that the thin carbon shell is permeable for molecules as large as calix[4]arene and, thus, will not hamper the mass transport of molecular oxygen. This high permeability is in agreement with previous studies on the carbon shell-encapsulated nanoparticles.[34] On the other hand, if the thickness of the shell increases, it becomes much harder for the reactant to reach the surface of the NPs, as depicted in Figure 3e.

Long-term stability of electrocatalyst is a critically important issue in electrochemical applications and fuel cell commercialization.[45] We conducted an accelerated durability test (ADT) under Ar for 10,000 potential cycles between 0.6 and 1.0 V vs RHE to test the stability of our nanocatalyst, and the results are shown in Figures 4a and 4b (for the full data set, see Figure S12 and S13). The data clearly reveal that ordered fct-PtFe/C exhibits superior long-term stability with negligible activity loss compared to Pt/C and disordered fcc-PtFe/C. Ordered fct-PtFe/C also shows good stability in ADT under O_2 saturated conditions (Figure 4b). According to cyclic voltammetry data, there is only little change in the current density of hydrogen underpotential deposition region (0–0.36 V) for ordered fct-PtFe/C after ADT both in Ar and O_2 conditions, indicating

DOI: 10.1021/jacs.5b09653
J. Am. Chem. Soc. 2015, 137, 15478–15485

small loss of the electrochemical surface area (Figure S12). On the other hand, disordered fcc-PtFe/C and Pt/C show significant decrease in the electrochemical surface area after ADT. For the long-term test under the full cell condition, we fabricated membrane electrode assembly (MEA), which is close to the realistic fuel cell operating condition, and performed continuous operation of 100 h (Figure 4c–4e). In this test, ordered fct-PtFe/C clearly demonstrates the higher stability with the loss in the maximum power density of only 3.4%. Compared to the loss of 27% observed from commercial Pt/C catalyst, this result demonstrates extremely high durability of our ordered fct-PtFe/C.

Structural analysis of ordered fct-PtFe nanocatalyst. In order to investigate the role of Pt–Fe alloy structures for the durability of nanocatalyst, we conducted *in situ* XANES measurements on Pt L_3-edge of ordered fct-PtFe/C, disordered fcc-PtFe/C, and Pt/C in Ar-saturated 0.1 M $HClO_4$ solution with the potential range from 0.6 to 1.2 V vs RHE. In these measurements, the extent of Pt oxidation is estimated by the whiteline intensity of XANES spectrum which reflects the amount of Pt d-band vacancy as a function of potential (Figure 5a, see Figure S15 for XANES spectra).[46,47] As mentioned above, oxidation of Pt atoms is one of the major deactivation mechanisms of the fuel cell electrocatalyst. By alloying with Fe, Pt atoms become more oxidation-resistive with the higher oxidation potentials than pure Pt.[48] According to the *in situ* XANES data, ordered fct-PtFe/C is more oxidation-resistant than the other two samples. Especially, comparing the PtFe/C samples measured after ADT, the extent of Pt oxidation of ordered fct-PtFe/C is less than half of that of disordered fcc-PtFe/C at 1.2 V. Considering that Pt atoms of Pt–Fe alloy become easier to be oxidized as more Fe atoms are dissolved from the alloy during ADT, we conclude that Fe atoms in ordered fct-PtFe structure are more stable and less dissolved than those in disordered fcc-PtFe. This hypothesis was tested by first-principles calculations on the stability of Fe atoms in ordered fct and disordered fcc structures, and the results are shown in Figure 5b (see Figures S16 and S17 and the corresponding text for details). In the calculation model, the vacancy formation energy, E_{vac}, is calculated for Fe atoms in the first and the second layer at the surface of PtFe alloy. In ordered fct structure, E_{vac} of Fe is 0.71 and 1.03 eV in the first and the second layer, respectively. On the other hand, in disordered fcc structure, E_{vac} have broad distribution with different Pt coordination numbers and chemical environments due to random arrangement of atoms. Interestingly, about half of the values of E_{vac} in both the first and the second layers of disordered fcc structure are lower than 0.71 and 1.03 eV, respectively. In other words, it is easier to remove some of Fe atoms from the surface of disordered fcc-PtFe than ordered fct-PtFe because their vacancy formation energy is lower than that of ordered fct-PtFe. Furthermore, the formation of Fe vacancies tends to further accelerate the dissolution of other remaining atoms.[49] As a result, the high stability of the fct-PtFe/C is attributed to its ordered intermetallic structure that rids of the broad distribution of E_{vac} generated by disordered atomic arrangement. Further experimental evidence of dissolution-resistive Fe atoms in ordered fct-PtFe is found from energy dispersive spectroscopy (EDS) analysis of the samples after 10,000 ADT cycles (Figure 5c). The elemental mapping images of Pt and Fe match well to STEM image of ordered fct-PtFe, indicating stable PtFe intermetallic structure of the NPs. In contrast, for disordered fcc-PtFe, the mapping image of Fe has

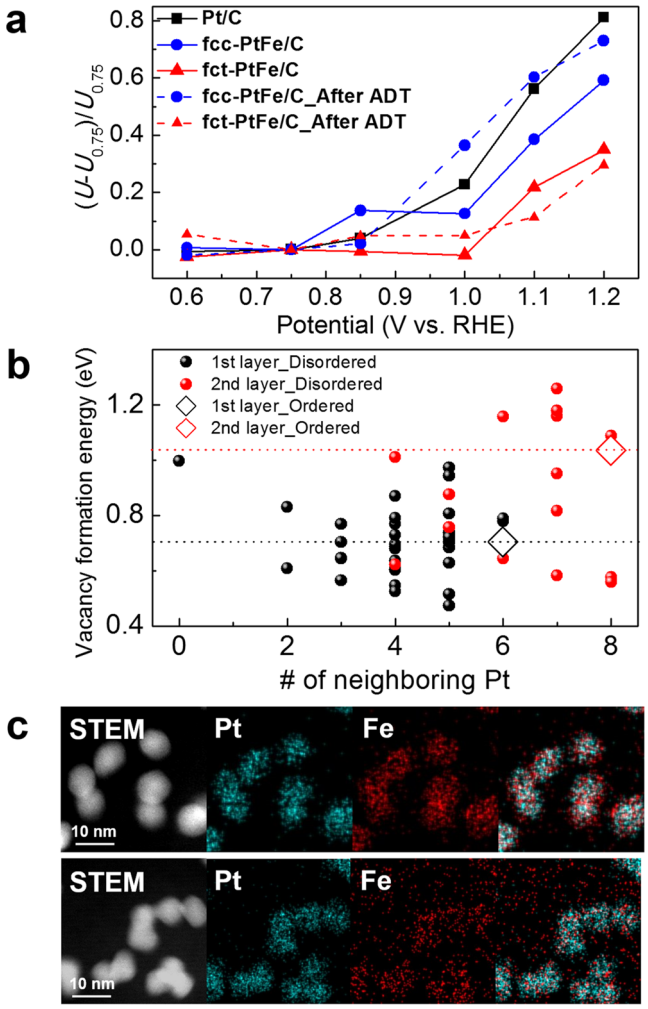

Figure 5. Long-term stability analysis through *in situ* XANES, computational analysis, and TEM. (a) Change in the whiteline intensity of the Pt L_3-edge as functions of potential measured by *in situ* XANES analysis. U and $U_{0.75}$ indicate the integrated whiteline intensity and the value of U at 0.75 V, respectively. (b) Vacancy formation energy E_{vac} of Fe calculated by first-principles calculations. The dashed lines indicate the values of E_{vac} for the first and the second layers of an ordered fct-PtFe structure. (c) HAADF-STEM and EDS elemental mapping analysis of ordered fct-PtFe/C (up) and disordered fcc-PtFe/C (down) after ADT 10,000 cycles.

no resemblance to either Pt mapping or STEM images. The atomic ratios of Pt and Fe from EDS data show that the amount of Fe in disordered fcc-PtFe is significantly decreased from Pt:Fe = 51:49 to 90:10 after ADT due to extensive dissolution of Fe, while the change in the atomic ratio of ordered fct-PtFe is minimal from 51:49 to 58:42 (see Table S3 for atomic ratios and Figure S18 for EDS line scan data of NPs). In addition to the contribution of ordered fct structure to the high durability, encapsulation by carbon shell not only provides physical barrier to prohibit the particle agglomeration but also stabilize the surface of the nanoparticles, both of which help to maintain the small size and high activity of the nanoparticles during the electrochemical reaction.[28] Our calculation data supports that the N-doped carbon shell encapsulating PtFe NPs can stabilize Pt-rich surface of the NPs due to strong adsorption of nitrogen to Pt atoms. Binding energies of Pt_{55}-cluster on N-doped graphene and undoped graphene were calculated as 5.46 and 3.73 eV, respectively

DOI: 10.1021/jacs.5b09653
J. Am. Chem. Soc. 2015, 137, 15478–15485

(Figure S19), showing that N-doped carbon shell can contribute to stabilize the surface of PtFe NPs.[28,32] Therefore, we conclude that the physical and chemical protection of N-doped carbon shell is responsible for the high stability in the long term operation.

CONCLUSION

In conclusion, we present a new and very effective approach to prepare highly active and stable fuel cell electrocatalyst by encapsulating carbon-supported PtFe NPs with a dual purpose N-doped carbon shell. This shell is *in situ* formed during thermal annealing of fcc-PtFe NPs to transform them into an ordered fct structure. The N-doped carbon shell not only prevents the coalescence of the NPs during a thermal annealing process to keep their sizes as small as ~6.5 nm but also protects them under harsh fuel cell operating conditions. We found that, when the thickness of the carbon shell is less than 1 nm, the shell is highly permeable so that the catalytic activity is not affected but the NPs are well protected. Our ordered fct-PtFe/C nanocatalyst coated with an N-doped carbon shell shows the higher performance compared to disordered fcc-PtFe/C and commercial Pt/C. Furthermore, ADT and MEA tests show that ordered fct-PtFe/C exhibits much higher long-term stability without significant activity loss. *In situ* XANES, EDS, and first-principles calculation studies reveal that an ordered fct-PtFe structure and the presence of an N-doped carbon shell are critical for the excellent performance of our nanocatalyst. We believe that this approach can open a new possibility for the development of high performance and cost-effective fuel cell catalysts in the near future.

EXPERIMENTAL SECTION

Synthesis. The synthesis of PtFe NPs was performed following the previously reported method (see the Supporting Information for the details).[27] As prepared PtFe NPs were loaded onto carbon black and the organic surfactant was removed by thermal treatment under air at 185 °C.[50] Polydopamine coating was carried out using a solution of dopamine hydrochloride with tris-HCl buffer (3 mg·ml^{-1}). The residual polydopamine was washed several times with ethanol and water. After drying the sample in vacuum oven at 80 °C overnight, thermal annealing was conducted at 700 °C for 2 h to obtain ordered fct-PtFe/C. For the preparation of disordered fcc-PtFe/C, carbon-loaded PtFe NPs were annealing at 400 °C without polydopamine coating.

Characterization. Bright field and energy-filtered TEM images were obtained on a JEOL-2200FS equipped with an image Cs-corrector and an Omega filter. The HADDF-STEM and EDS measurements were performed on a JEM-ARM200F and JEOL-2100F equipped with a Cs-corrector. All TEM instruments were operated at 200 kV. HRPD, HR-PES, and *in situ* XANES measurements were performed at Pohang Accelerator Laboratory (PAL) 9B beamline (λ = 1.4970 Å), 8A1 beamline ($h\nu$ = 630 eV), and 8C beamline. The details on the synchrotron X-ray measurements are provided in the Supporting Information.

Electrochemical method. Electrochemical experiments were conducted in 0.1 M $HClO_4$ at 293 K using a conventional three-compartment electrode system with an Autolab rotating disc electrode (RDE) and Autolab 302 potentiostat. A RDE electrode with 0.196 cm^2 area glassy carbon electrode was used as working electrode. Saturated calomel electrode and Pt wire were used as reference and counter electrodes, respectively. All of the potentials are versus the reversible hydrogen electrode (RHE). Ink was prepared by mixing nanocatalyst, Nafion ionomer and 2-isopropanol. After sonication, ink was deposited onto the glassy carbon electrode and dried to form a uniform film. The Pt loading level was 7.8 μg cm^{-2} in PtFe alloy nanoparticles and 16.0 μg cm^{-2} in commercial Pt/C (Johnson Matthey Co., 20 wt %).

ASSOCIATED CONTENT

Supporting Information

The Supporting Information is available free of charge on the ACS Publications website at DOI: 10.1021/jacs.5b09653.

Experimental details related to the material synthesis, electrochemistry, computational analysis details, and full cell analysis. Physical analysis such as TEM, XPS, and XAFS and results of nanoparticles and electrochemical results such as CV and EIS results. (PDF)

AUTHOR INFORMATION

Corresponding Authors

*ysung@snu.ac.kr.
*thyeon@snu.ac.kr.

Author Contributions

#D.Y.C. and S.W.J. equally contributed to this work.

Notes

The authors declare no competing financial interest.

ACKNOWLEDGMENTS

This work was supported by the Institute for Basic Science (IBS) in Korea (IBS-R006-D1, IBS-R006-G1, and IBS-R006-Y1).

REFERENCES

(1) Jung, N.; Chung, D. Y.; Ryu, J.; Yoo, S. J.; Sung, Y. E. *Nano Today* **2014**, *9*, 433−456.
(2) Lim, B.; Jiang, M.; Camargo, P. H. C.; Cho, E. C.; Tao, J.; Lu, X.; Zhu, Y.; Xia, Y. *Science* **2009**, *324*, 1302−1305.
(3) Chen, C.; Kang, Y.; Huo, Z.; Zhu, Z.; Huang, W.; Xin, H. L.; Snyder, J. D.; Li, D.; Herron, J. A.; Mavrikakis, M.; Chi, M.; More, K. L.; Li, Y.; Markovic, N. M.; Somorjai, G. A.; Yang, P.; Stamenkovic, V. R. *Science* **2014**, *343*, 1339−1343.
(4) Zhang, S.; Hao, Y.; Su, D.; Doan-Nguyen, V. V. T.; Wu, Y.; Li, J.; Sun, S.; Murray, C. B. *J. Am. Chem. Soc.* **2014**, *136*, 15921−15924.
(5) Guo, S.; Zhang, S.; Sun, S. *Angew. Chem., Int. Ed.* **2013**, *52*, 8526−8544.
(6) Stephens, I. E. L.; Bondarenko, A. S.; Grønbjerg, U.; Rossmeisl, J.; Chorkendorff, I. *Energy Environ. Sci.* **2012**, *5*, 6744−6762.
(7) Huang, X.; Zhao, Z.; Cao, L.; Chen, Y.; Zhu, E.; Lin, Z.; Li, M.; Yan, A.; Zettl, A.; Wang, Y. M.; Duan, X.; Mueller, T.; Huang, T. *Science* **2015**, *348*, 1230−1234.
(8) Zhang, L.; Roling, L. T.; Wang, X.; Vara, M.; Chi, M.; Liu, J.; Choi, S. − I.; Park, J.; Herron, J. A.; Xie, Z.; Mavrikakis, M.; Xia, Y. *Science* **2015**, *349*, 412−416.
(9) Wu, J.; Yang, H. *Acc. Chem. Res.* **2013**, *46*, 1848−1857.
(10) Porter, N. S.; Wu, H.; Quan, Z.; Fang, J. *Acc. Chem. Res.* **2013**, *46*, 1867−1877.
(11) You, H.; Yang, S.; Ding, B.; Yang, H. *Chem. Soc. Rev.* **2013**, *42*, 2880−2904.
(12) Wang, D.; Li, Y. *Adv. Mater.* **2011**, *23*, 1044−1060.
(13) Bing, Y.; Liu, H.; Zhang, L.; Ghosh, D.; Zhang, J. J. *Chem. Soc. Rev.* **2010**, *39*, 2184−2202.
(14) Zhang, L.; Iyyamperumal, R.; Yancey, D. F.; Crooks, R. M.; Henkelman, G. *ACS Nano* **2013**, *7*, 9168−9172.
(15) Ferreira, P. J.; La O, G. J.; Shao-Horn, Y.; Morgan, D.; Makharia, R.; Kocha, S.; Gasteiger, H. A. *J. Electrochem. Soc.* **2005**, *152*, A2256−A2271.
(16) Tang, L.; Han, B.; Persson, K.; Friesen, C.; He, T.; Sieradzki, K.; Ceder, G. *J. Am. Chem. Soc.* **2010**, *132*, 596−600.
(17) Kim, J.; Lee, Y.; Sun, S. *J. Am. Chem. Soc.* **2010**, *132*, 4996−4997.
(18) Wang, D.; Xin, H. L.; Hovden, R.; Wang, H.; Yu, Y.; Muller, D. A.; Disalvo, F. J.; Abruña, H. D. *Nat. Mater.* **2013**, *12*, 81−87.

DOI: 10.1021/jacs.5b09653
J. Am. Chem. Soc. 2015, 137, 15478−15485

(19) Kang, Y.; Pyo, J. B.; Ye, X.; Gordon, T. R.; Murray, C. B. *ACS Nano* **2012**, *6*, 5642−5647.
(20) Li, Q.; Wu, L.; Wu, G.; Su, D.; Lv, H.; Zhang, S.; Zhu, W.; Casimir, A.; Zhu, H.; Mendoza-Garcia, A.; Sun, S. *Nano Lett.* **2015**, *15*, 2468−2473.
(21) Ghosh, T.; Vukmirovic, M. B.; DiSalvo, F. J.; Adzic, R. R. *J. Am. Chem. Soc.* **2010**, *132*, 906−907.
(22) Wang, D.; Yu, Y.; Xin, H. L.; Hovden, R.; Ercius, P.; Mundy, J. A.; Chen, H.; Richard, J. H.; Muller, D. A.; Disalvo, F. J.; Abruña, H. D. *Nano Lett.* **2012**, *12*, 5230−5238.
(23) Wang, G.; Huang, B.; Xiao, L.; Ren, Z.; Chen, H.; Wang, D.; Abruña, H. D.; Lu, J.; Zhuang, L. *J. Am. Chem. Soc.* **2014**, *136*, 9643−9649.
(24) Rong, C. B.; Li, D.; Nandwana, V.; Poudyal, N.; Ding, Y.; Wang, Z. L.; Zeng, H.; Liu, J. P. *Adv. Mater.* **2006**, *18*, 2984−2988.
(25) Lee, D. C.; Mikulec, F. V.; Pelaez, J. M.; Koo, B.; Korgel, B. *J. Phys. Chem. B* **2006**, *110*, 11160−11166.
(26) Chen, H.; Wang, D.; Yu, Y.; Newton, K. A.; Muller, D. A.; Abruña, H.; Disalvo, F. J. *J. Am. Chem. Soc.* **2012**, *134*, 18453−18459.
(27) Holby, E. F.; Sheng, W.; Shao-Horn, Y.; Morgan, D. *Energy Environ. Sci.* **2009**, *2*, 865−871.
(28) Guo, L.; Jiang, W. J.; Zhang, Y.; Hu, J. S.; Wei, Z. D.; Wan, L. J. *ACS Catal.* **2015**, *5*, 2903−2909.
(29) Cheng, N.; Banis, M. N.; Liu, J.; Riese, A.; Li, X.; Li, R.; Ye, S.; Knights, S.; Sun, X. *Adv. Mater.* **2015**, *27*, 277−281.
(30) Baldizzone, C.; Mezzavilla, S.; Carvalho, H. W. P.; Meier, J. C.; Schuppert, A. K.; Heggen, M.; Galeano, C.; Grunwaldt, J. D.; Schüth, F.; Mayrhofer, K. J. J. *Angew. Chem., Int. Ed.* **2014**, *53*, 14250−14254.
(31) Galeano, C.; Meier, J. C.; Peinecke, V.; Bongard, H.; Katsounaros, I.; Topalov, A. A.; Lu, A.; Mayrhofer, K. J. J.; Schüth, F. *J. Am. Chem. Soc.* **2012**, *134*, 20457−20465.
(32) Pylypenko, S.; Borisevich, A.; More, K. L.; Corpuz, A. R.; Holme, T.; Dameron, A. A.; Olson, T. S.; Dinh, H. N.; Gennett, T.; O'Hayre, R. *Energy Environ. Sci.* **2013**, *6*, 2957−2964.
(33) Zhang, S.; Zhang, X.; Jiang, G.; Zhu, H.; Guo, S.; Su, D.; Lu, G.; Sun, S. *J. Am. Chem. Soc.* **2014**, *136*, 7734−7739.
(34) Liu, R.; Mahurin, S. M.; Li, C.; Unocic, R. R.; Idrobo, J. C.; Gao, H.; Pennycook, S. J.; Dai, S. *Angew. Chem., Int. Ed.* **2011**, *50*, 6799−6802.
(35) Lee, H.; Dellatore, S. M.; Miller, W. M.; Messersmith, P. B. *Science* **2007**, *318*, 426−430.
(36) Stamenkovic, V. R.; Fowler, B.; Mun, B. S.; Wang, G.; Ross, P. N.; Lucas, C. A.; Markovic, N. M. *Science* **2007**, *315*, 493−497.
(37) Hwang, S. J.; Kim, S. K.; Lee, J. G.; Lee, S. C.; Jang, J. H.; Kim, P.; Lim, T. H.; Sung, Y. E.; Yoo, S. J. *J. Am. Chem. Soc.* **2012**, *134*, 19508−19511.
(38) Kim, Y. S.; Jeon, S. H.; Bostwick, A.; Rotenberg, E.; Ross, P. N.; Stamenkovic, V. R.; Markovic, N. M.; Noh, T. W.; Han, S.; Mun, B. S. *Adv. Energy Mater.* **2013**, *3*, 1257−1261.
(39) Strasser, P.; Koh, S.; Anniyev, T.; Greeley, J.; More, K.; Yu, C.; Liu, Z.; Kaya, S.; Nordlund, D.; Ogasawara, H.; Toney, M. F.; Nilsson, A. *Nat. Chem.* **2010**, *2*, 454−460.
(40) Min, M. K.; Cho, J.; Cho, K.; Kim, H. *Electrochim. Acta* **2000**, *45*, 4211−4217.
(41) Wu, G.; More, K. L.; Johnston, C. M.; Zelenay, P. *Science* **2011**, *332*, 443−447.
(42) Chung, H. T.; Won, J. H.; Zelenay, P. *Nat. Commun.* **2013**, *4*, 1922−1925.
(43) Genorio, B.; Strmcnik, D.; Subbaraman, R.; Tripkovic, D.; Karapetrov, G.; Stamenkovic, V. R.; Pejovnik, S.; Marković, N. M. *Nat. Mater.* **2010**, *9*, 998−1003.
(44) Genorio, B.; Subbaraman, R.; Strmcnik, D.; Tripkovic, D.; Stamenkovic, V. R.; Markovic, N. M. *Angew. Chem., Int. Ed.* **2011**, *50*, 5468−5472.
(45) Debe, M. K. *Nature* **2012**, *486*, 43−51.
(46) Zhang, J.; Sasaki, K.; Sutter, E.; Adzic, R. R. *Science* **2007**, *315*, 220−222.
(47) Friebel, D.; Miller, D. J.; Nordlund, D.; Ogasawara, H.; Nilsson, A. *Angew. Chem., Int. Ed.* **2011**, *50*, 10190−10192.
(48) Stamenkovic, V. R.; Mun, B. S.; Arenz, M.; Mayrhofer, K. J. J.; Lucas, C. A.; Wang, G.; Ross, P. N.; Markovic, N. M. *Nat. Mater.* **2007**, *6*, 241−247.
(49) Wei, G. F.; Liu, Z. P. *Energy Environ. Sci.* **2011**, *4*, 1268−1272.
(50) Li, D.; Wang, C.; Tripkovic, D.; Sun, S.; Markovic, N. M.; Stamenkovic, V. R. *ACS Catal.* **2012**, *2*, 1358−1362.

DOI: 10.1021/jacs.5b09653
J. Am. Chem. Soc. 2015, 137, 15478−15485